Chin. J. Astron. Astrophys. Vol. 7 (2007), No. 1, 81–90
(*http://www.chjaa.org*)

Chinese Journal of
Astronomy and
Astrophysics

A Statistical Analysis of Point-like Sources in the *Chandra* Galactic Center Survey *

J. F. Wu[1,†], S. N. Zhang[1,2], F. J. Lu[2] and Y. K. Jin[3]

[1] Department of Physics and Center for Astrophysics, Tsinghua University, Beijing 100084
jfwu03@mails.tsinghua.edu.cn
[2] Key Laboratory of Particle Astrophysics, Institute of High Energy Physics, Chinese Academy of Sciences, Beijing 100049
[3] Department of Engineering Physics and Center for Astrophysics, Tsinghua University, Beijing 100084

Received 2006 April 21; accepted 2006 June 16

Abstract The *Chandra* Galactic Center Survey detected ~ 800 X-ray point-like sources in the $2^\circ \times 0.8^\circ$ sky region around the Galactic Center. We study the spatial and luminosity distributions of these sources according to their spectral properties. Fourteen bright sources detected are used to fit jointly an absorbed power-law model, from which the power-law photon index is determined to be $\sim$2.5. Assuming that all other sources have the same power-law form, the relation between hardness ratio and HI column density $N_{\rm H}$ is used to estimate the $N_{\rm H}$ values for all sources. Monte Carlo simulations show that these sources are more likely concentrated in the Galactic center region, rather than distributed throughout the Galactic disk. We also find that the luminosities of the sources are positively correlated with their HI column densities, i.e., a more luminous source has a higher HI column density. From this relation, we suggest that the X-ray luminosity comes from the interaction between an isolated old neutron star and interstellar medium (mainly dense molecular clouds). Using the standard Bondi accretion theory and the statistical information of molecular clouds in the Galactic center, we confirm this positive correlation and calculate the luminosity range in this scenario, which is consistent with the observation ($10^{32} - 10^{35}$ erg s^{-1}).

Key words: methods: data analysis — Galaxy: center — X-ray: stars

1 INTRODUCTION

The central regions of galaxies are usually crowded with many celestial bodies of different physical properties. The center of our Galaxy is an ideal laboratory to study X-ray sources and the related high energy astrophysical processes. It has been the observational target of most X-ray satellites, such as *ROSAT* (Snowden et al. 1997; Sidoli, Belloni & Meregetti 2001), *ASCA* (Sakano et al. 2002) and *BeppoSAX* (Sidoli et al. 1999). In these observations many X-ray point-like sources are detected. The *ROSAT* survey covered a $3^\circ \times 4^\circ$ sky region around the Galactic Center and detected 107 X-ray point-like sources in 0.1–2.4 keV. In *ASCA* observations, 52 point-like sources were detected. *BeppoSAX* has also observed 16 X-ray point-like sources in the central region of our Galaxy. *Chandra X-ray Observatory* (*CXO*) has a much better spatial resolution (0.5 arcsec) than the previous satellites (e.g. *ROSAT* 20 arcsec). It can produce high quality images of the Galactic center. The *Chandra* Galactic Center Survey (hereafter GCS) was carried out in July, 2001

* Supported by the National Natural Science Foundation of China.

† Current Address: Dept. of Astronomy & Astrophysics, The Pennsylvania State University, 525 Davey Lab, University Park, PA 16802, USA; jfwu@astro.psu.edu

(Wang, Gotthelf & Lang 2002), which consists of 30 separate ACIS-I observations (Obs. ID 2267–2296, energy band 0.2–10.0 keV) with a total exposure time of 94.2 hours (~ 340 ks), covers $2^\circ \times 0.8^\circ$, about $280\,\mathrm{pc} \times 110\,\mathrm{pc}$ (taking the distance of Galactic center to be 8.0 kpc). About 800 point-like sources were detected.

A variety of analyses to explore the nature of these discrete sources have been done. Pfahl, Rappaport & Podsiadlowski (2002) discussed the possibility of the $Chandra$ GCS sources being wind-accreting neutron stars, while Belczynski & Taam (2004) introduced another possibility of the low luminosity ($10^{31} - 10^{32}$ erg s^{-1}) sources being Roche lobe overflow accretion systems. Belczynski & Taam (2004) also argued that accreting neutron star systems are not likely to be the majority of the sources. Multiwavelength observations have been proposed on these sources to further explore the nature of these sources. ChaMPlane (*Chandra* Multiwavelength Plane Survey, Grindlay et al. 2005) focuses on the multiwavelength observations of the $Chandra$ X-ray sources in the Galactic plane and bulge. They employed X-ray and optical surveys, a follow up spectroscopy and an infrared identification. Their recent results (Laycock et al. 2005) showed that high mass X-ray binaries (HMXBs) are not the dominant population (fewer than 10%) of the X-ray sources in the Galactic center. Bandyopadhyay et al. (2005) made an infrared survey on parts of the $Chandra$ GCS region. Analysis on potential counterparts indicated that the sources may be accreting X-ray binaries. Recently, Liu & Li (2005) carried out an evolutionary population synthesis study on discrete sources in the Galactic center region. Their results showed neutron star low mass X-ray binaries could not account for most sources in Wang et al. (2002) survey. Muno et al. (2006) reanalysed the data of *Chandra* GCS and suggested that a major part of these sources could be cataclysmic variables (CVs) since the local Galactic neighborhood X-ray sources showed a CV population in the $10^{32} - 10^{34}$ erg s^{-1} luminosity range.

Despite of extensive work done previously, the nature of X-ray sources in the Galactic center is still not understood completely. Our work presented here is a statistical analysis of the sources in Wang's $Chandra$ GCS, including their spatial distribution and flux characteristics. In Section 2, the method of data analysis and the results are described in detail, including spectral fitting and parameter determination. In Section 3, the spatial distribution of the sources is discussed. In Section 4 another potential nature of GCS X-ray sources is proposed and in Section 5 a summary is given.

2 SPECTRAL FITTING & $N_{\rm H}$ DETERMINATION

Chandra has excellent angular resolution. Although many GCS sources have only a few counts, the background counts are even much lower. So for most sources the detection probability is close to unity. The efficiency correction is ignored here because the luminosity function of these sources is not discussed in this paper.

The *psextract* procedure in the CIAO package is used to obtain the spectral files of the sources. The regions we used to extract energy spectra are circles chosen to contain all source photons, while minimizing the effect of nearby sources and background. The radii of these circles range from 6 to 24 pixels. The background region is made of several circles of similar radii. The spectra are re-binned to make each energy channel to have no fewer than 25 counts for most sources, while for other sources with smaller counts, each energy channel to have no fewer than 10 counts. Then the *Xspec* in Heasoft package is used to fit the spectra with the absorbed power-law model, i.e., "phabs(po)" model in *Xspec*. There are three parameters in this model — the photon spectral index Γ, the neutral hydrogen column density $N_{\rm H}$ and the normalization factor A. Because the effective exposure time for each field is short, the total counts for sources without significant pileup are not sufficient for a high quality spectral fitting, in a simultaneous determination of $N_{\rm H}$ and Γ for each source; many other sources are also too faint for any meaningful spectral fitting individually. We therefore chose 14 sources, each with total counts of more than 80 and without significant pileup (the largest pileup in these 14 sources is 8%). We assume that all sources have a similar value of Γ, attributing the different hardness ratios of these sources to different values of $N_{\rm H}$. Our goal is to search for one value of Γ that best describes all the14 sources. Spectral fittings of these 14 sources show their power-law photon indices $\sim 2 - 3$, indicating soft spectral properties. Γ values were tried from 1.5 to 3.5 at steps of 0.2. For each trial value of Γ, i.e., we fit the absorbed power-law model by fixing Γ, and obtained one value of chi-squared. This was done for all the different trials values of Γ. We then find that $\Gamma = 2.5$ gives the smallest chi-squared value (Fig. 1), with a reduced chi-squared value of about 1.180 for 185 degrees of freedom. We thus conclude that $\Gamma = 2.5^{+0.9}_{-0.5}$ for a 68.3% confidence interval. We believe this single photon

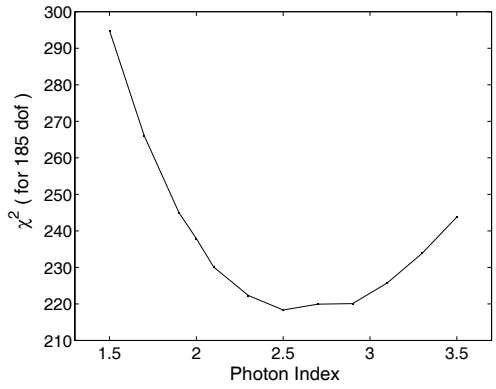

Fig. 1 Total chi-squared values for different photon indices. When Γ=2.5, the reduced chi-squared value is most close to 1.

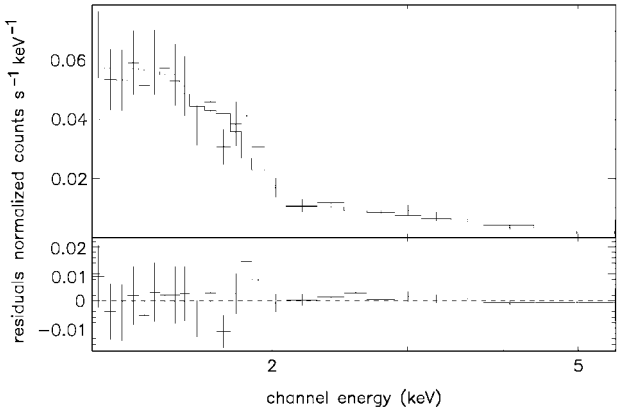

Fig. 2 Fitted spectrum of CXO J174417.2–293945: $N_{\rm H} = (0.5476 \pm 0.0876) \times 10^{22}$ cm^{-2}, Γ=2.5.

index can describe most of the GCS sources adequately with no obvious selection effects, because these 14 sources are distributed through the whole $N_{\rm H}$ distribution acquired below (Fig. 4). Figure 2 is an example of spectral fitting. Table 1 shows the spectral fitting results for these 14 sources with the photon index fixed at 2.5.

Assuming that $\Gamma = 2.5$ for all sources, the $N_{\rm H}$ value for each source can be estimated according to the hardness ratios of the source. Following the definitions of Wang (private communication): HR= $\frac{b-a}{b+a}$ and HR2= $\frac{c-b}{c+b}$, where $a,\ b$ and c are the counts [1] in three bands: A (1–3 keV), B (3–5 keV) and C (5–8 keV). The values of HR and HR2 for each source are given in the source list. Using the PIMMS software (*http://cxc.harvard.edu/toolkit/pimms.jsp*), the relation between HI column density $N_{\rm H}$ and hardness ratios can be obtained as shown in Figure 3. Here we should emphasize that the definitions of hardness ratios in Figure 3, labelled as HR' and HR2', are different from the ones above, HR and HR2. This is because when using PIMMS we can only obtain the values of count rates, i.e., the parameters of Poisson processes in the three bands $\lambda_A,\ \lambda_B,\ \lambda_C$: Their definitions are HR$' = \frac{\lambda_B-\lambda_A}{\lambda_B+\lambda_A}$ and HR2$' = \frac{\lambda_C-\lambda_B}{\lambda_C+\lambda_B}$.

[1] An off-angle efficiency correction has been applied. However, the maximum correction factor for the 8.638 keV photons at 8' off-axis angle is only 1.67. Therefore, the corrected counts still follow Poisson distribution closely.

Table 1 Fitting results of 14 *Chandra* GCS sources ($\Gamma = 2.5$)

Obs.ID	Source	Counts	$N_{\rm H}(10^{22}{\rm cm}^{-2})$	χ^2/dof
2271	J174722.9-280904	108	16.81 ± 1.101	16.926/21
2273	J174639.1–285351	179	$(1.464 \pm 0.378) \times 10^{-4}$	21.616/14
2273	J174622.7–285218	119	15.02 ± 2.732	18.401/11
2274	J174705.4–280859	141	0.2518 ± 0.2823	8.073/12
2275	J174319.4–291359	133	1.234 ± 0.2266	10.669/11
2276	J174550.4–284921	180	5.534 ± 0.641	29.323/19
2276	J174550.4–284911	86	4.989 ± 1.992	6.515/5
2277	J174804.9–282917	94	14.92 ± 3.407	4.583/6
2277	J174729.0–283516	204	0.8724 ± 0.2423	23.174/14
2278	J174417.3–293944	695	0.7984 ± 0.0907	26.578/24
2282	J174602.2–291039	174	1.759 ± 0.252	18.668/16
2285	J174626.1–282530	158	4.640 ± 0.616	13.99/13
2294	J174502.8–282505	107	0.621 ± 0.250	12.533/11
2295	J174451.7–285309	104	3.703 ± 0.655	6.66/8

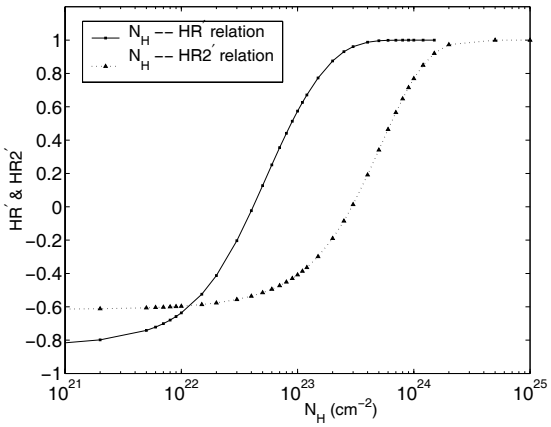

Fig. 3 Relation between $N_{\rm H}$ and HR$'$, HR2$'$. The solid line with squares is the relation of $N_{\rm H}$ and HR$'$, while the dotted line with triangles is the one of $N_{\rm H}$ and HR2$'$.

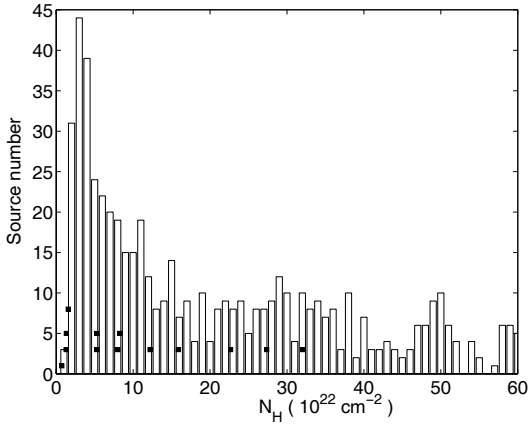

Fig. 4 $N_{\rm H}$ distribution of *Chandra* GCS sources. The black squares mark the 13 sources used for determining their joint photon index (Sec. 2, one of the 14 sources cannot give the $N_{\rm H}$ value using our method). Since their $N_{\rm H}$ values span across almost the whole range, it is believed there is no selection effect involved.

We therefore use the method in Jin et al. (2006) to estimate the values and error intervals of HR $'$ and HR2$'$. For a Poisson process, the λ parameter obeys the Gamma distribution under certain counts as

$$p(\lambda_A = x | n_A = a) \; = \; \frac{x^a e^{-x}}{a!}. \tag{1}$$

Based on this result, the probability density function of λ_A/λ_B is,

$$p\Big(\frac{\lambda_A}{\lambda_B} = z | n_A = a, n_B = b\Big) \; = \; \frac{z^a (a+b+1)!}{(z+1)^{a+b+2} a! b!}. \tag{2}$$

The expectation of λ_A/λ_B is

$$E\Big(\frac{\lambda_A}{\lambda_B} | n_A = a, n_B = b\Big) \; = \; \frac{a+1}{b}. \tag{3}$$

The most probable value z_0 can be obtained as

$$z_0 \;=\; \frac{a}{b+2}. \tag{4}$$

Hence, for a Poisson process, λ_A/λ_B is not exactly equal to a/b. Here the most probable value is taken as the estimate of λ_A/λ_B. For the hardness ratio defined as HR$'$ $= \frac{\lambda_B-\lambda_A}{\lambda_B+\lambda_A}$, the probability density function is

$$p\Big(\frac{\lambda_B-\lambda_A}{\lambda_B+\lambda_A}=z|n_A=a,n_B=b\Big) \;=\; \frac{(1-z)^a(1+z)^b(a+b+1)!}{2^{(a+b+1)}a!b!}. \tag{5}$$

Again the most probable value z_0 is taken as the estimate of $\frac{\lambda_B-\lambda_A}{\lambda_B+\lambda_A}$,

$$z_0=\Big(\frac{\lambda_B-\lambda_A}{\lambda_B+\lambda_A}\Big)_{\rm peak} \;=\; \frac{b-a}{b+a}. \tag{6}$$

The method of error estimation is shown by the following equation (the error interval is denoted by [C, D]),

$$\int_{\rm C}^{z_0} p\Big(\frac{\lambda_B-\lambda_A}{\lambda_B+\lambda_A}=z\Big){\rm d}z \;=\; 90\%\times\int_{-1}^{z_0} p\Big(\frac{\lambda_B-\lambda_A}{\lambda_B+\lambda_A}=z\Big){\rm d}z, \tag{7}$$

$$\int_{z_0}^{\rm D} p\Big(\frac{\lambda_B-\lambda_A}{\lambda_B+\lambda_A}=z\Big){\rm d}z \;=\; 90\%\times\int_{z_0}^{1} p\Big(\frac{\lambda_B-\lambda_A}{\lambda_B+\lambda_A}=z\Big){\rm d}z. \tag{8}$$

According to the relations in Figure 3, the $N_{\rm H}$ values and errors for each source can be derived by linear interpolation. As can be seen from Figure 3, HR$'$ and HR2$'$ estimates are more accurate for $N_{\rm H} < 2\times10^{23}$ cm^{-2} and $N_{\rm H} > 2\times10^{23}$ cm^{-2}, respectively; and the $N_{\rm H}$ value for each source is assigned accordingly. Because the curves in Figure 3 cannot cover the whole range of HR$'$ and HR2$'$ of $[-1,1]$, the $N_{\rm H}$ values of nearly 80% (~ 600) of the GCS sources are acquired in this way; these are used in the following investigation. The $N_{\rm H}$ distributions derived from HR' and HR2' are shown in Figure 4.

3 SPATIAL DISTRIBUTION OF GCS SOURCES

3.1 Angular Distribution

Figure 5 shows the angular distribution of these sources. For angular distance in the $(0.25\,^\circ, 0.30^\circ)$ interval, there are the largest number of sources. However, on the source number density curve the Galactic center is the densest region. A sharp decrease exists immediately outside the center. Further out, at angular distances $> 0.1^\circ$ the decrease of the source number density slows down, and the overall decrease is slower than an exponential decrease.

3.2 Radial Distribution — Where are the sources?

Our goal is to find the three dimensional distribution of these sources from the projected two dimensional image. It is natural to consider that the sources are likely concentrated in the Galactic center region since that region is known to be crowded by various kinds of objects. Another possibility is that the major part of the sources are distributed throughout the Galactic disk. Here Monte Carlo simulation is used to study which model is consistent with the statistical properties of these sources.

We start with Figure 6. The horizontal axis of this figure is the HI column density, and the vertical axis is the unabsorbed flux in 0.2–10.0 keV (all the fluxes hereafter are in the same energy band), calculated from the $\Gamma = 2.5$ power-law model, the corresponding HI column density and the count rate of each source. The blank region in the bottom right corner reflects the sensitivity of the survey. The criterion of the source detection is based on Poisson probability (Wang 2004). The probability of a count deviation above the background $C_{\rm bg}$ can be formulated as

$$P = 1-\sum_{n=0}^{C_{\rm tl}-1}\frac{C_{\rm bg}^n}{n!}e^{-C_{\rm bg}}, \tag{9}$$

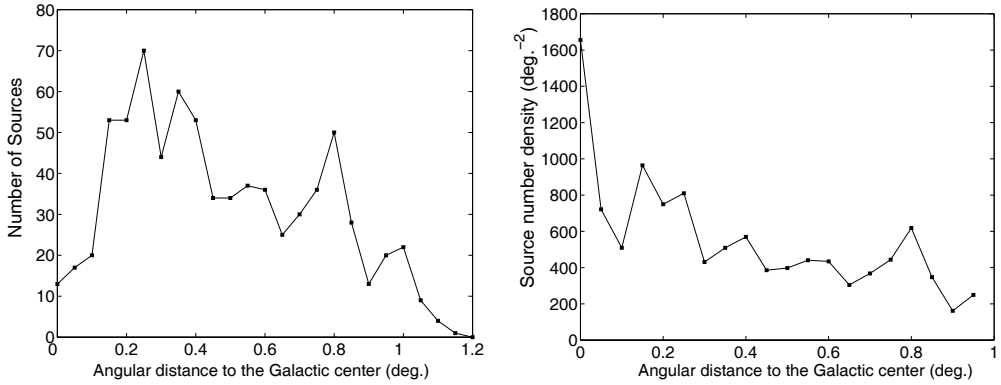

Fig. 5 Angular distribution of *Chandra* GCS sources. Left panel: source count in intervals of angular distance, $[0^\circ, 0.05^\circ)$, $[0.05^\circ, 0.10^\circ)$ ... $[1.20^\circ, 1.25^\circ)$; Right panel: source number density in intervals of angular distance, $[0^\circ, 0.05^\circ)$, $[0.05^\circ, 0.10^\circ)$ ... $[0.95^\circ, 1.00^\circ)$.

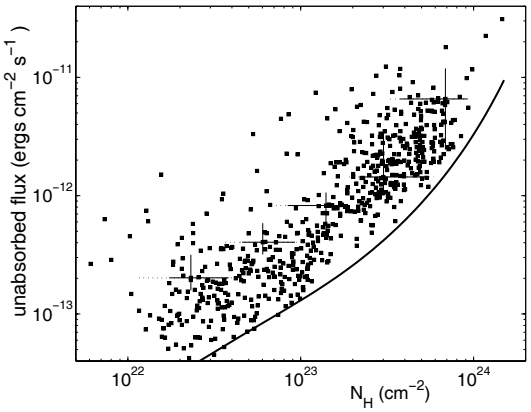

Fig. 6 Correlation of unabsorbed flux of X-ray sources with HI column density. The bold line shows the detection threshold of this survey. The five crosses stand for the scales of the error bars of $N_{\rm H}$ and flux values. The extended dotted lines show the $N_{\rm H}$ error intervals if the source photon indices Γ vary in $2 \sim 3$ range.

where $C_{\rm tl}$ and $C_{\rm bg}$ are the total counts and background counts for each source, respectively. If the probability P is less than a preset threshold $P_{\rm th}$, then we have a source detection. Here in this *Chandra* GCS, $P_{\rm th}$ is set at 10^{-5}. In our case, this threshold can be approximated by $S/N > 2$, where $S/N = (C_{\rm tl} - C_{\rm bg})/\sqrt{C_{\rm tl}}$. This point can be seen in the following simulations. The bold curve in Figure 6 shows the detection threshold in the approximation.

We designed some simulated observations. We assumed a set of sources with a certain luminosity function, and had them either spread on the disk or concentrated at the Galactic center. The parameters in the simulation are: 1) cumulative luminosity function: power-law with $\Gamma = 0.5$, which is similar to the discrete X-ray sources in nearby spiral galaxies (e.g. Colbert et al. 2004; Tennant et al. 2001); 2) HI column density distribution: For the case of central concentration, we simply took a uniform distribution, thus minimizing the number of parameters; for the case of a spread out distribution, the HI column density was assumed to be proportional to the radial distance, starting with 1×10^{23} cm^{-2} at the centre (corresponding to 8.0 kpc distance (Baganoff et al. 2003)), up the assumed farthest boundary of the Milky Way at 30.0 kpc; 3) a background count distribution, the same Poisson distribution as in the *Chandra* GCS observation.

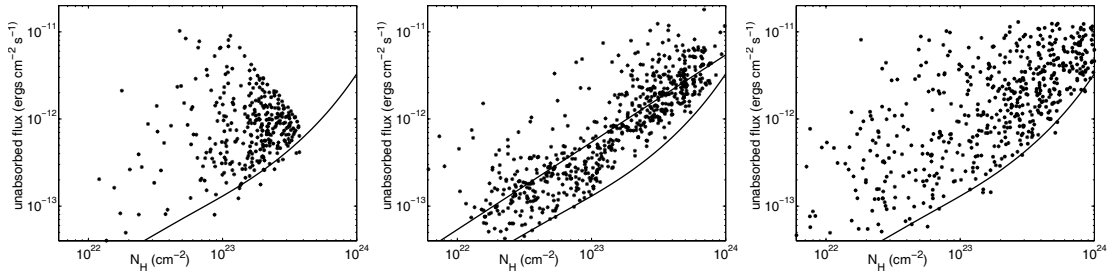

Fig. 7 HI column density vs unabsorbed flux, where the bold curve in all three panels marks the detection threshold of the real survey. *Left panel:* simulation with sources uniformly spread out over the Galactic disk and an HI column density proportional to the radial distance. *Middle panel:* the real *Chandra* survey. *Right panel:* simulation with most sources concentrated in the Galactic center and a uniformly distributed HI column density.

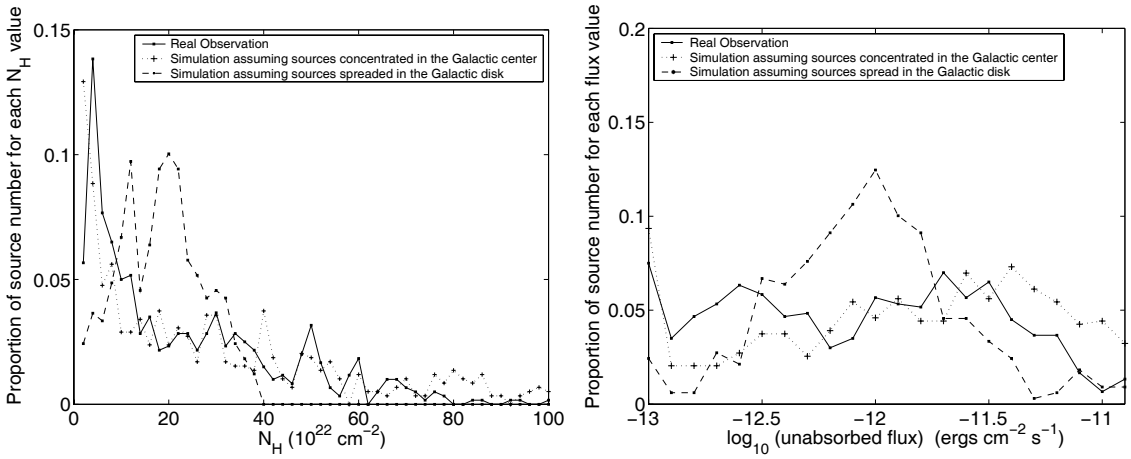

Fig. 8 *Left panel:* Comparison of $N_{\rm H}$ value distributions in the real observation and the two simulations. The simulation with central concentration of sources is closer to the observation. The main difference shows up in the low $N_{\rm H}$ value intervals. *Right panel:* Comparison of unabsorbed flux value distributions in the real observation and the two simulations. Again the simulation with central concentration of sources is the more likely one. The first point stands for all unabsorbed fluxes $< 10^{-13}$ erg cm^{-2} s^{-1}, the last point stands for all unabsorbed fluxes $> 10^{-11}$ erg cm^{-2} s^{-1}.

Figures 7 and 8 summarize the simulation results. Here χ^2 test is used to find out which simulation is closer to the observation. For two discrete data sets, R_i and S_i, over a number ν of intervals, the χ^2 value is defined by the following equation (Press et al. 1992),

$$\chi^2 = \sum_i \frac{(\sqrt{S/R}R_i - \sqrt{R/S}S_i)^2}{R_i + S_i}, \tag{10}$$

$$R \equiv \sum_i R_i, \qquad S \equiv \sum_i S_i. \tag{11}$$

and the degree of freedom of the χ^2 distribution is ν.

First, we examine the case that X-ray sources are spread out in the disk. Figure 8 shows that the simulated HI column density distribution and the unabsorbed flux distribution in this case are very different

from those of the observation: $\chi^2/\mathrm{dof} = 199/40$ for the $N_{\rm H}$ distribution, $\chi^2/\mathrm{dof} = 126/22$ for the unabsorbed flux distribution. The main disagreement is that there are too many sources with HI column density at $2 \times 10^{23} - 4 \times 10^{23}$ cm^{-2} in this simulation than in the observation. The reason is that the source number density does not vary with the Galactic latitude, i.e., the number density is uniform in the field of view. However, the density of the Galactic material is known to decrease in high latitude regions. An exponentially decreasing factor $\exp(-z/z_0)$ is then used. For smaller z_0 value, the χ^2/dof value is found to decrease: even for $z_0 \sim 1$ pc, the simulated distribution of HI column density cannot satisfactorily match the observation ($\chi^2/\mathrm{dof} = 111/40$). Such small value of z_0 is inconsistent with our knowledge of Galactic mass distribution: for various kinds of matter, $z_0 \sim 70 - 400$ pc (Ferrière 2001). The mass model of the Milky Way (Bahcall & Soneira 1980; Dehnen & Binney 1998; Grimm, Gilfanov & Sunyaev 2002) is also tested and again the simulation cannot match the observation ($\chi^2/\mathrm{dof} = 294/40$ for the $N_{\rm H}$ distribution). Furthermore, there are many differences between the left panel and middle panel of Figure 7. A void appears in the top right part of the simulation figure which is not present in the observation. The reason for this void is that for the same luminosity range the flux of a farther source is smaller. There is no reason to believe that the farther sources are more luminous. Therefore, this difference cannot be accounted for easily. In fact we find that this kind of void exists whether or not we add the exponentially decreasing factor. We thus conclude it is not likely that the sources in $Chandra$ GCS are distributed throughout the Galactic disk.

Now, we examine the other case: Point-like sources concentrated in the Galactic center. The HI column density distribution is assumed to be a uniform distribution. Comparisons with the observed HI column density and flux distributions are: $\chi^2/\mathrm{dof} = 104/40$ and $\chi^2/\mathrm{dof} = 83/22$, indicating significant improvement over the previous case of spread-out distribution. However, even this case does not match the real observation completely. The middle and right panels of Figure 7 show the differences. One major difference is on the top left part of the two panels. In the observation, there is a void on the top left part, i.e., fewer high flux sources with small HI column density are detected than in the simulation, which cannot be explained by selection effect, since selection effect only makes sources under the threshold curve undetectable. Therefore, based on this finding we infer that some kind of positive correlation exists between the HI column density and the unabsorbed flux, i.e., brighter sources have a higher HI column densities. Since these sources are probably concentrated in the Galactic center, they should have approximately the same distances. We therefore conclude that a positive correlation exists between the X-ray luminosities and HI column densities of the Galactic center sources.

4 A POTENTIAL INTERPRETATION FOR THE NATURE OF THESE SOURCES

As shown in the previous section, the luminosity of the X-ray sources is positively correlated with the HI column density. One possibility is that the X-ray luminosity comes from the interaction between an isolated neutron star and interstellar medium (ISM), mainly in the form of dense molecular clouds in the Galactic center region.

Since stars in the Galactic center are very old, there should be many dead isolated neutron stars, which may move into the molecular clouds with speeds $\sim 10^2$ km s^{-1} (Arzoumanian et al. 2002), and then accrete the ISM via standard Bondi accretion. The statistical properties of molecular clouds in the Galactic center region (Miyazaki & Tsuboi 2000; Oka et al. 2001) are as follows: 1) mass M: 1.3×10^4–1.3×10^8 $M_\odot$; 2) size R: 1.3–50 pc; 3) mass density ρ: 10^{-22}–10^{-18} g cm^{-3}; 4) number density n: 10^2–10^6 cm^{-3}. The sound speed of the molecular clouds ($\sim 1 - 10$ km s^{-1}) is much smaller than the velocity of the moving neutron star. The accretion rate of standard Bondi accretion should be calculated as

$$\dot{M} \sim \frac{4\pi (GM_n)^2 m_p n}{(V^2 + C_S^2)^{3/2}} \sim 10^9 n V_7^{-3} \ \mathrm{g\ s^{-1}}, \tag{12}$$

where V_7 is the velocity of neutron star in units of 10^7 cm s^{-1}. We take $V_7 = 1$, neutron star mass $M_n = 1.4\ M_\odot$, neutron star radius $R_n = 10$ km, then the accretion luminosity is

$$L_{\rm acc} \sim \frac{GM_n\dot{M}}{R_n} \sim 10^{29} n \ \mathrm{erg\ s^{-1}}. \tag{13}$$

Substitute the number density of molecular clouds into the above equation, the luminosity should be 10^{31} – 10^{35} erg s^{-1}. For the *Chandra* GCS sources studied above, the unabsorbed fluxes stay in the range of 10^{-14}–10^{-11} erg cm^{-2} s^{-1}. If most of these sources are at the Galactic center at a distance of 8.0 kpc, the luminosities should be $10^{32} - 10^{35}$ erg s^{-1}, consistent with our result. The values of column density from the center to the border of the dense molecular clouds are 10^{22}–10^{24} cm^{-2}. Thus for the neutron stars in the molecular clouds, the HI column density should be in this range. Since the molecular clouds have different volumes, the HI column density is not strictly proportional to the number density of the molecular cloud. However, a positive correlation should exist. For sources with small HI column density, they are not likely to have high accreting X-ray luminosity. Therefore, in this scenario the luminosity of X-ray sources is positively correlated with the HI column density as in the observation. The top left void in the middle panel of Figure 7 can thus be explained in this scenario.

From the discussion above, we also argue that the absorption of X-ray is mainly caused by the dense molecular clouds near the Galactic center, rather than by the Galactic disk ISM along the line of sight to us. In fact, using the ISM model of the Milky Way (Ferrière 1998, eqs. (6) and (7)) the HI column density from the Galactic center to us is calculated as only $\sim 10^{22}$ cm^{-2}, only a small fraction of the HI column density of *Chandra* GCS sources. Our model can also explain why the HI column density of sources in the Galactic center varies over a wide range. The HI column density of foreground sources should be $< 10^{22}$ cm^{-2}. We can see in Figure 6 that the foreground sources are only a small part of the whole catalog. The percentage of background extragalactic sources is also very small (Bandyopadhyay et al. 2005). Thus the contribution from foreground and background sources can be ignored.

Treves et al. (2000) reviewed the theory and the observations of old isolated neutron stars in the Milky Way. They estimated that there should be 10^8–10^9 neutron stars in our Galaxy, and most of them are dead. The Galactic center region is thus a good place to observe old isolated neutron stars. Neutron stars in this region are so old that the rotation frequency and magnetic field have decayed and the neutron stars could be accretors, instead of ejectors and propellers. Even in ejector or propeller phase, accretion could also occur (Zhang, Yu & Zhang 1998): A small portion of materials accretes onto the polar region of the neutron star through a quasi-spherical Advection Dominated Accretion Flow (ADAF). This scenario may occur in neutron star soft X-ray transients. For our model, the accretion onto isolated neutron stars can also produce variability due to instability of magnetic field or fine structure of the ISM (Treves, private communication).

For those neutron stars that are still alive (i.e. radio pulsars), there can also exist a positive correlation between their X-ray luminosity and the ISM density. As these neutron stars move into ISM with a speed much higher than the ISM sound speed, there should be a bow shock. Romani, Cordes & Yadigaroglu (1997) discussed the Guitar nebula formed in this scenario. The shock luminosity from the shocked ISM along the Guitar body is proportional to the hydrogen number density. Recent research on bow shocks also showed that for some region of the shock, the X-ray luminosity is positively correlated with the ISM density (Gaensler et al. 2004).

Further study on the nature of point-like X-ray sources needs multiwavelength observation. Bandyopadhyay et al. (2005) took a VLT infrared survey on 77 X-ray sources of the *Chandra* GCS field. They detected candidate counterparts for 75% of the sources in their sample, and suggested that the X-ray sources might be wind-fed accreting neutron star binaries. However, their sample is only a small part of the sources. Laycock et al. (2005) (ChaMPlane program) excluded High Mass X-ray Binaries (HXMBs) as the main contributor of X-ray sources in the Galactic center. Other kinds of sources account for more than 90% of the X-ray sources. Furthermore, Belczynski & Taam (2004) argued that accreting neutron star systems are not likely to be the main contributor to the faint X-ray sources in the Galactic center, because neither wind-fed nor Roche lobe accreting neutron star systems can explain the amount or the spectral properties of the sources in survey catalogs in Wang, Gotthelf & Lang (2002). Our model of the X-ray sources and old isolated neutron stars with Bondi accretion, can explain the faint soft X-ray source population in the Galactic center.

5 SUMMARY

We have performed statistical analysis on 600 of ~ 800 point-like sources detected in the Galactic center survey of *Chandra X-ray Observatory*, thanks to its excellent spatial resolution and broad energy range. Fourteen bright sources detected are used to fit jointly an absorbed power-law model, from which the power-

law photon index is determined to be $\sim$2.5. Assuming that all other sources have the same power-law form, we use the relation between hardness ratio and HI column density $N_{\rm H}$ to estimate the $N_{\rm H}$ values for all sources. We study the spatial distribution of these sources with Monte Carlo simulations and infer that these sources are mainly concentrated in the Galactic center region. The luminosities of X-ray sources are found to be positively correlated with the HI column density. We propose a model of old isolated neutron star with Bondi accretion as the X-ray sources to explain the correlation, which is consistent with the present knowledge of dense molecular clouds in the Galactic center. We argue that the molecular clouds should be the main contributor to X-ray absorption, rather than the ISM in the Galactic disk. Further extensive multiwavelength surveys are needed to study the nature of X-ray sources in the Galactic center further.

Acknowledgements We thank Dr. Q. D. Wang of University of Massachusetts for providing the GCS point-like source list prior to its publication and his useful discussions and suggestions. We also thank J.-L. Han, Y. Shen, F. Y. Bian, D. Lai, A. Treves, S. M. Tang and W. M. Zhang for helpful discussions. X. Chen read the manuscript carefully and gave many helpful suggestions, especially on English writing. This study is supported in part by the Special Funds for Major State Basic Research Projects and by the National Natural Science Foundation of China (grant No. 10521001).

References

Arzoumanian Z., Chernoff D. F., Cordes J. M., 2002, ApJ, 568, 289
Baganoff F. K., Maeda Y., Morris M. et al., 2003, ApJ, 591, 891
Bahcall J. N., Soneira R. M., 1980, ApJS, 44, 73
Bandyopadhyay R. M., Miller-Jones J. C. A., Blundell K. M. et al, 2005, MNRAS, 364, 1195
Belczynski K., Taam R. E., 2004, ApJ, 616, 1159
Colbert E. J. M., Heckman T. M., Ptak A. F., 2004, ApJ, 602, 231
Dehnen W., Binney J., 1998, MNRAS, 294, 429
Ferrière K. M., 1998, ApJ, 497, 759
Ferrière K. M., 2001, Rev. Mod. Phys., 73, 1031
Gaensler B. M., van der Swaluw E., Camilo F. et al., 2004, ApJ, 616, 383
Grimm H.-J., Gilfanov M., Sunyaev R., 2002, A&A, 391, 923
Grindlay J. E., Hong J., Zhao P. et al, 2005, ApJ, 635, 920
Jin Y. K., Zhang S. N., Wu J. F., 2006, ApJ, 653, 1566
Laycock S., Grindlay J., van den Berg M. et al., 2005, ApJ, 634, L53
Miyazaki A., Tsuboi M., 2000, ApJ, 536, 357
Muno M. P., Bauer F. E., Bandyopadhyay R. M. et al., 2006, ApJS, 165, 173
Liu X.-W., Li X.-D., 2006, A&A, 449, 135
Oka T., Hasegawa T., Sato F. et al., 2001, ApJ, 562, 348
Pfahl E., Rappaport S., Podsiadlowski P., 2002, ApJ, 571, L37
Press W. H., Flannery B. P., Teukolsky S. A. et al., 1992, Numerical Recipes in C: The Art of Scientific Computing, Cambridge: Cambridge University Press, Second edition, §14.3
Romani R. W., Cordes J. M., Yadigaroglu I.-A., 1997, ApJ, 484, L137
Sakano M., Koyama K., Murakami H. et al., 2002, ApJS, 138, 19
Sidoli L., Mereghetti S., Israel G. L. et al., 1999, ApJ, 525, 215
Sidoli L., Belloni T., Mereghetti S., 2001, A&A, 368, 835
Snowden S. L., Egger R., Freyberg M. J. et al., 1997, ApJ, 485, 125
Tennant A. F., Wu K., Ghosh K. K. et al., 2001, ApJ, 549, L43
Treves A., Turolla R., Zane S. et al., 2000, PASP, 112, 297
Wang Q. D., Gotthelf E. V., Lang C. C., 2002, Nature, 415, 148
Wang Q. D., 2004, ApJ, 612, 159
Zhang S. N., Yu W., Zhang W., 1998, ApJ, 494, L71